Supplement of Biogeosciences, 16, 3247–3266, 2019
https://doi.org/10.5194/bg-16-3247-2019-supplement

Biogeosciences Open Access EGU

Supplement of

Attribution of N_2O sources in a grassland soil with laser spectroscopy based isotopocule analysis

Erkan Ibraim et al.

Correspondence to: Erkan Ibraim (erkan.ibraim@empa.ch)

1. N_2O fluxes with coupled flux chambers and GC-ECD

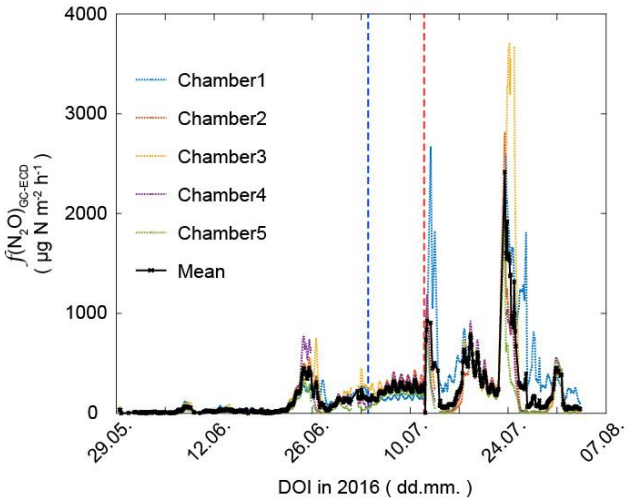

SI Figure 1 N_2O fluxes at the intensively managed grassland site De-Fen determined with five automated chambers and N_2O analysis by GC-ECD. Vertical dashed lines indicate the mowing (blue) and the manure applications (red).

1.1. Comparison of N_2O mole fractions and N_2O emission rates

N_2O concentrations 2 m above ground analysed by TREX-QCLAS show a significant correlation (p-value < 0.05) with $f(N_2O)$ obtained with the coupled flux-chamber and GC-ECD (SI Figure 2).

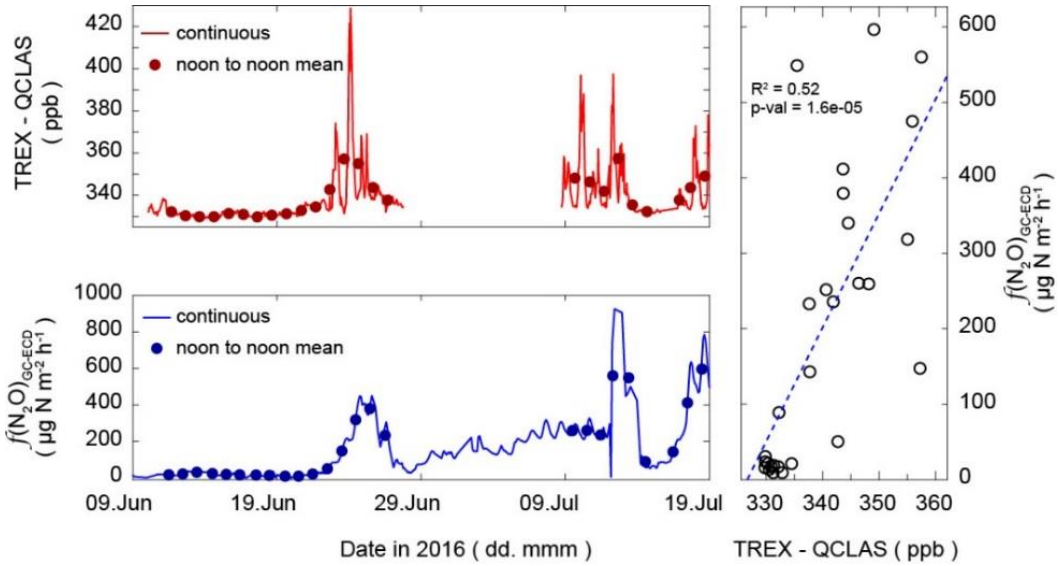

SI Figure 2 Comparison of N_2O mole fractions measured with the TREX-QCLAS system and the N_2O fluxes measured with the coupled flux-chambers and GC-ECD system. The figure on the right depicts the comparison of noon-to-noon average values as obtained with the two measurement systems shown on the left. The r-squared value and the p-value are given.

2. Source signatures

2.1. Miller and Tans (2003) analysis

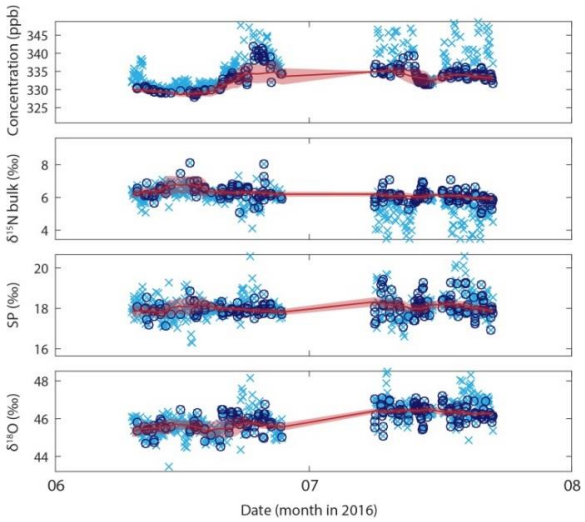

SI Figure 3 Background N_2O mixing ratios and isotopic composition used for the Miller-Tans analysis. Pale blue crosses represent all data points; points falling within the lowest 5% of a moving 1-day window were used for the baseline retrieval (dark blue circles). The 5-day smoothed background is shown in red with the shaded region indicating 1 standard deviation.

A Miller and Tans (2003) analysis as performed by Harris et al. (2017) was conducted to retrieve source signatures with a independent method in order to verify the Keeling (1958, 1961) plot-derived results. For the first third of the measurement period source signatures calculated with the Keeling (1958, 1961) plot approach did not pass the selection criteria due to lack of N_2O build up and Miller and Tans (2003) derived source signatures are rather scattered. In periods with reasonable N_2O fluxes, there is a very good agreement between the two methods.

2.2. Illustratory example for the SP vs. $\Delta\delta^{15}N^{bulk}$ and SP vs. $\Delta\delta^{18}O$ plots

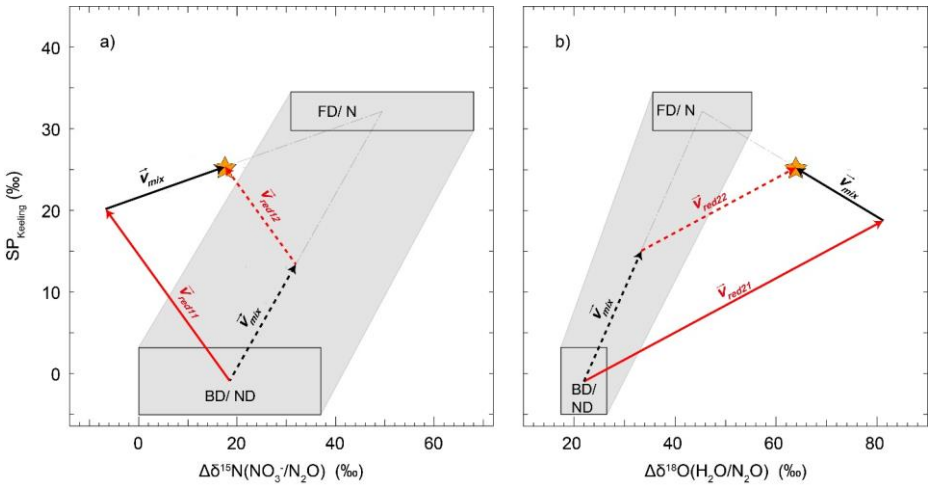

SI Figure 4 Illustration of the two concepts behind the two mapping approaches used in the main document. The source signatures of fungal denitrification- and nitrification-derived N_2O (FD/ N) and bacterial denitrification- and nitrifier denitrification-derived N_2O (BD/ ND) are indicated with rectangles according to the values given in Table 4. The shaded area represents the mixing region of the two domains. As exemplary values, the average source signatures for our measurements are given with the orange star. Red arrows denote the path of partial N_2O reduction to N_2, while black arrows indicate the direction of mixing with FD/ N-derived N_2O. Solid arrows indicate scenario 1 (first reduction, then mixing), while dashed arrows indicate scenario 2 (first mixing, then reduction). (a) SP versus $\Delta\delta^{15}N$ map according to Koba et al. (2009), where $\Delta\delta^{15}N = \delta^{15}N\text{-}NO_3^- - \delta^{15}N\text{-}N_2O$ (b) SP versus $\Delta\delta^{18}O$ of soil-emitted N_2O according to Lewicka-Szczebak et al. (2017), where $\Delta\delta^{18}O = \delta^{18}O\text{-}N_2O - \delta^{18}O\text{-}H_2O$.

SI Figure 4 illustrates the SP vs. $\Delta\delta^{15}N^{bulk}$ and SP vs. $\Delta\delta^{18}O$ plots with the average source signatures (given as orange stars). The two rectangles labelled with FD/ N and BD/ ND indicate the expected source signatures of fungal denitrification/ nitrification (FD/ N) derived N_2O and bacterial denitrification/ nitrifier-denitrification (BD/ ND) derived N_2O. Source signatures falling into the grey shaded area correspond to a N_2O mainly derived by a mix of the two process domains. Red arrows indicate the path of source-signature changes due to partial N_2O reduction, while black arrows indicate source signature changes due to mixing of N_2O originating from the two process domains. In principle, two scenarios are possible to interpret the measured source signatures (Lewicka-Szczebak et al., 2017). Scenario 1: BD/ ND derived N_2O is partially reduced to N_2, then the residual N_2O is mixed with FD/ N derived N_2O. Scenario 2: BD/ ND derived N_2O is mixed with FD/ N derived N_2O first and then partial N_2O reduction to N_2 occurs. The rate of N_2O reduction is calculated with the Rayleigh approach (described in detail in the main manuscript), while the rate of mixing is assumed linearly proportional to the length of the mixing vectors (v_{mix}).

2.3. N_2O-to-N_2 reduction rates of individual events determined with different approaches and using different scenarios

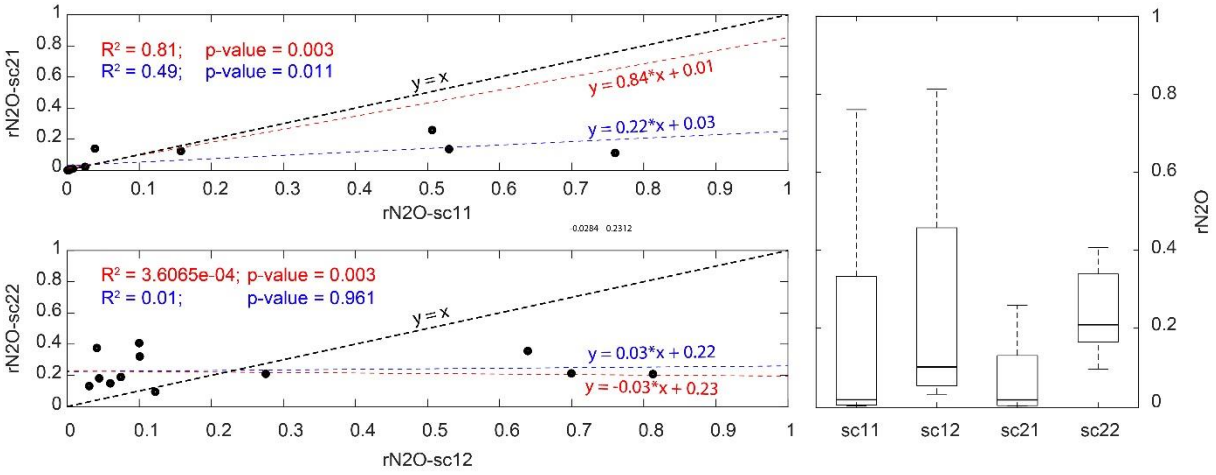

SI Figure 5 Left: Fraction of remaining N_2O after the N_2O reduction as estimated with different approaches and assuming different scenarios (rN_2O refers to residual N_2O after N_2O reduction to N_2; sc11 = Koba approach scenario 1, sc12 = Koba approach scenario 2, sc21 = Lewicka-Szczebak approach scenario 1, and sc22 = Lewicka-Szczebak approach scenario 2). Dashed lines correspond to the 1:1 line. While the blue fit corresponds to the linear regression of all data points (n=12), the red fit was carried out only for rN2O values smaller than 0.4, i.e. for cases with high N_2O reduction rates. Right: distribution of the rN2O values given with boxplots.

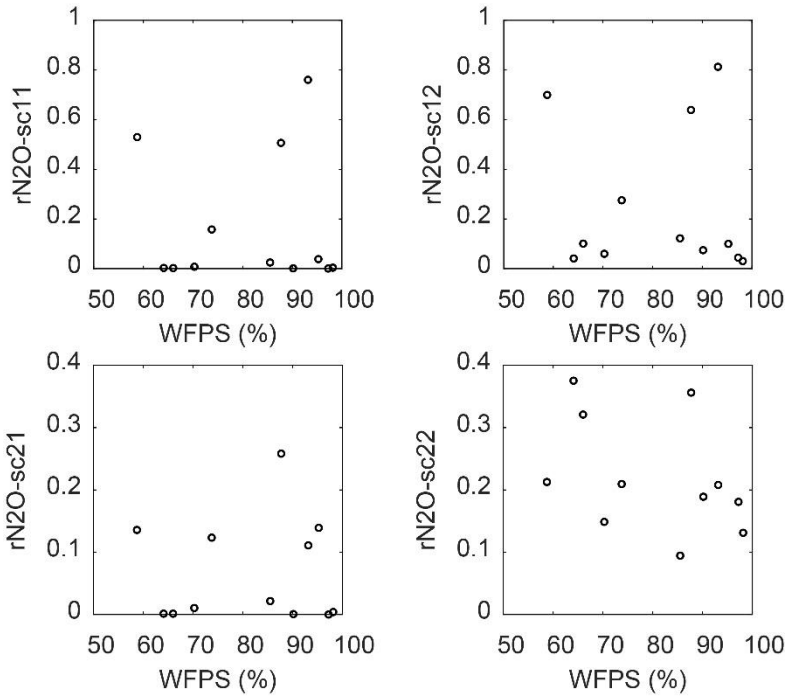

SI Figure 6 Fraction of remaining N_2O after N_2O reduction plotted against WFPS, where rN_2O has been calculated using different approaches and assuming different scenarios (rN_2O refers to residual N_2O after N_2O reduction to N_2. Explanation of suffix: sc11 = Koba approach scenario 1, sc12 = Koba approach scenario 2, sc21 = Lewicka-Szczebak approach scenario 1, and sc22 = Lewicka-Szczebak approach scenario 2)

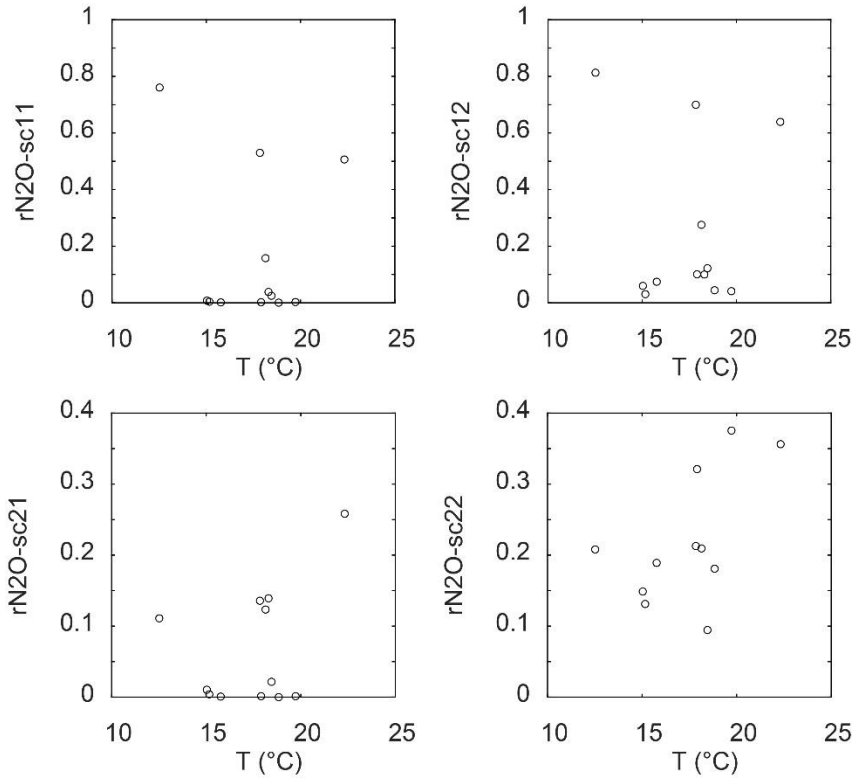

SI Figure 7 Fraction of remaining N_2O after N_2O reduction plotted against ambient temperature, where rN_2O has been calculated using different approaches and assuming different scenarios (rN_2O refers to residual N_2O after N_2O reduction to N_2. Explanation of suffix: sc11 = Koba approach scenario 1, sc12 = Koba approach scenario 2, sc21 = Lewicka-Szczebak approach scenario 1, and sc22 = Lewicka-Szczebak approach scenario 2)

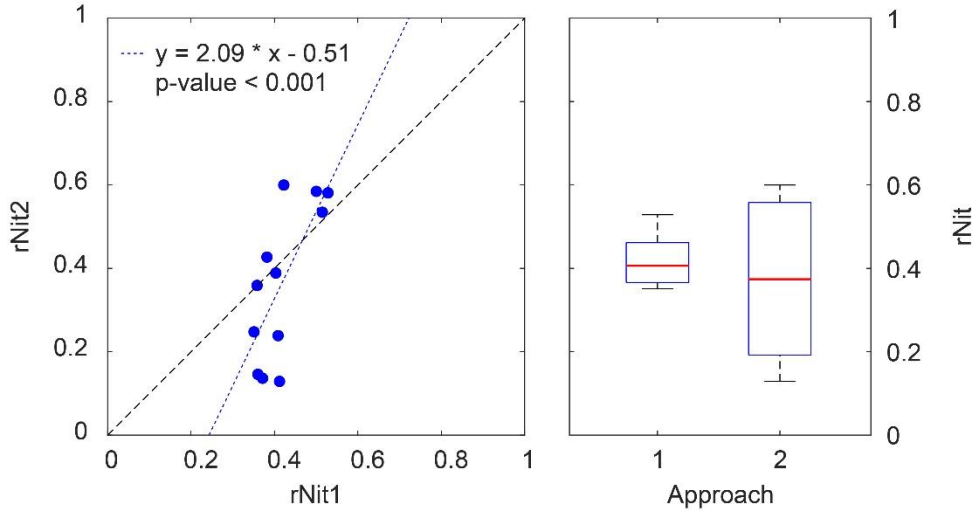

SI Figure 8 left: Fraction of N_2O originating from fungal denitrification or nitrification (rNit), determined based on the mapping approach according to Lewicka-Szczebak et al. (2017) (rNit2; referred to as approach 2) versus rNit as determined based on the mapping approach according to the Koba et al. (2009) approach (rNit1; referred to as approach 1). Right: boxplots of rNit1 and rNit2. The medians of rNit1 and rNit2 are 0.37 and 0.41, respectively, indicating 37 and 41 % of FD/N derived N_2O on the total emissions.

2.4. Contribution of FD/ N and BD/ ND to the total emissions

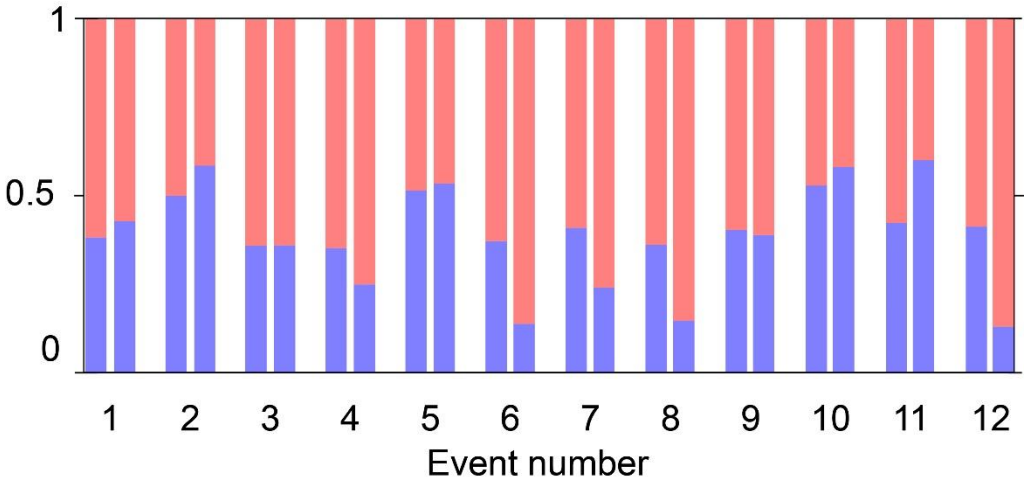

SI Figure 9 Blue bars indicate the fraction of FD/ N derived N_2O on the total N_2O emissions for individual emission events, while red bars refer to the fraction of BD/ND derived N_2O.

3. FLEXPART-COSMO simulations with local micro meteorological inputs

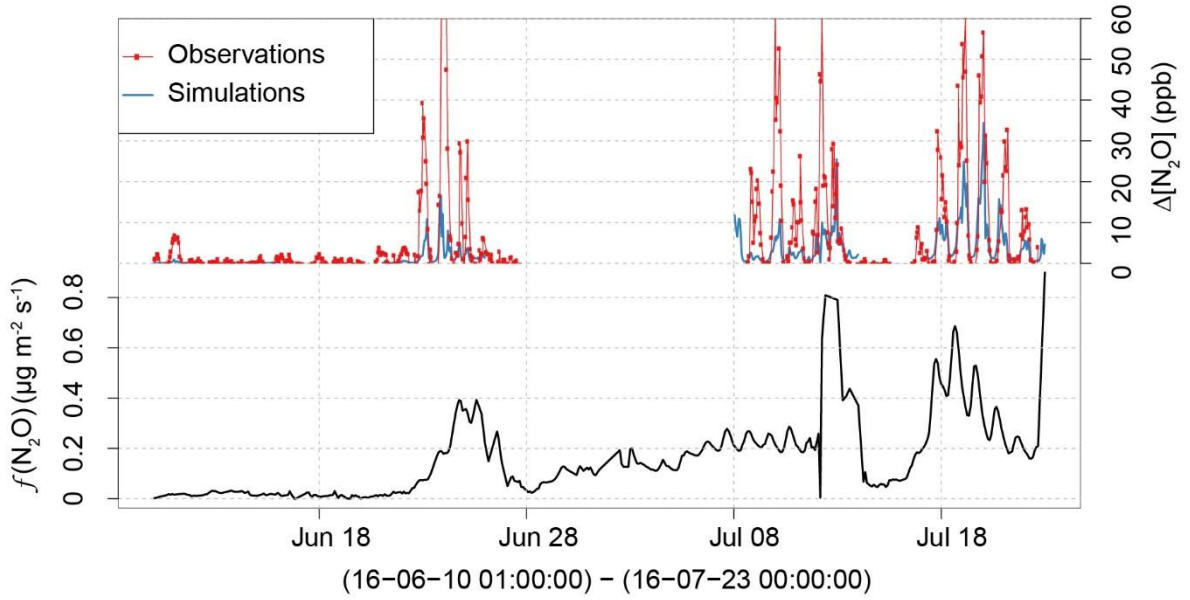

SI Figure 10 Simulation of concentration accumulation events with FLEXPART-COSMO. Observation data were obtained with TREX-QCLAS (black), while Sim Local (red) and Sim Nest (green) refer to values simulated with FLEXPART-COSMO assuming horizontally homogenous fluxes of $f(N_2O)$ in the local domain shown in Figure 1 and in a larger domain (16 km x 16 km), respectively. Fluxes were taken as the mean flux observed in the chamber measurements as shown in the lower panel.

3.1. Footprints of individual events

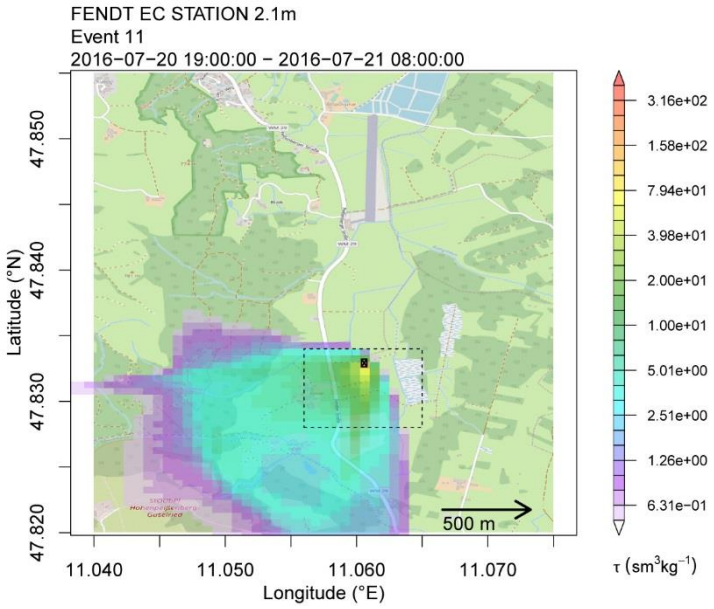

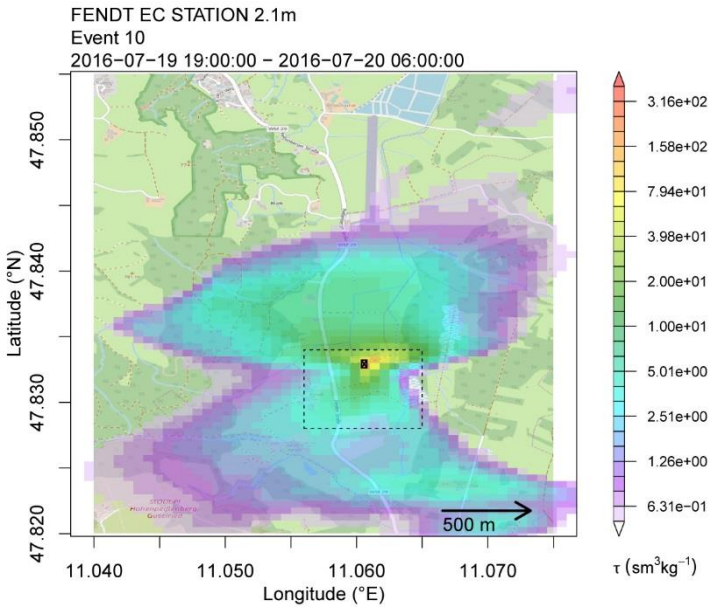

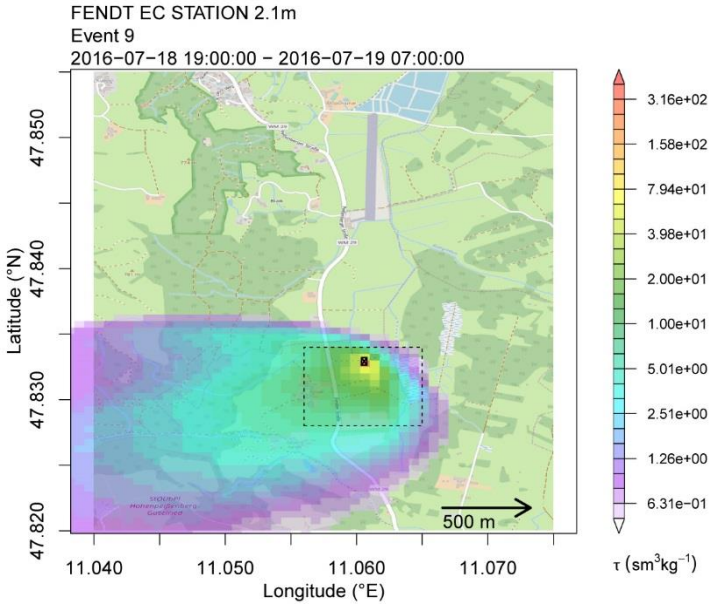
FENDT EC STATION 2.1m
Event 9
2016-07-18 19:00:00 – 2016-07-19 07:00:00
Latitude (°N)
47.820
47.830
47.840
47.850
11.040
11.050
11.060
11.070
Longitude (°E)
500 m
3.16e+02
1.58e+02
7.94e+01
3.98e+01
2.00e+01
1.00e+01
5.01e+00
2.51e+00
1.26e+00
6.31e-01
τ (sm3kg-1)

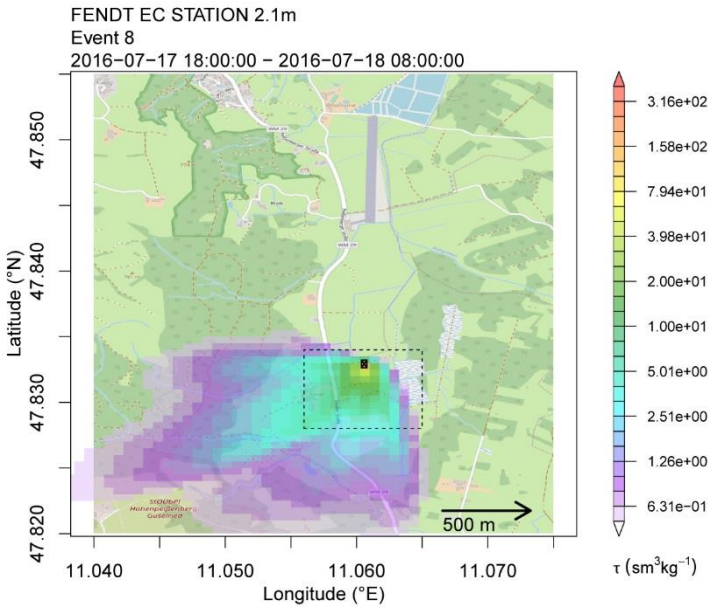
FENDT EC STATION 2.1m
Event 8
2016-07-17 18:00:00 – 2016-07-18 08:00:00
Latitude (°N)
47.820
47.830
47.840
47.850
11.040
11.050
11.060
11.070
Longitude (°E)
500 m
3.16e+02
1.58e+02
7.94e+01
3.98e+01
2.00e+01
1.00e+01
5.01e+00
2.51e+00
1.26e+00
6.31e-01
τ (sm3kg-1)

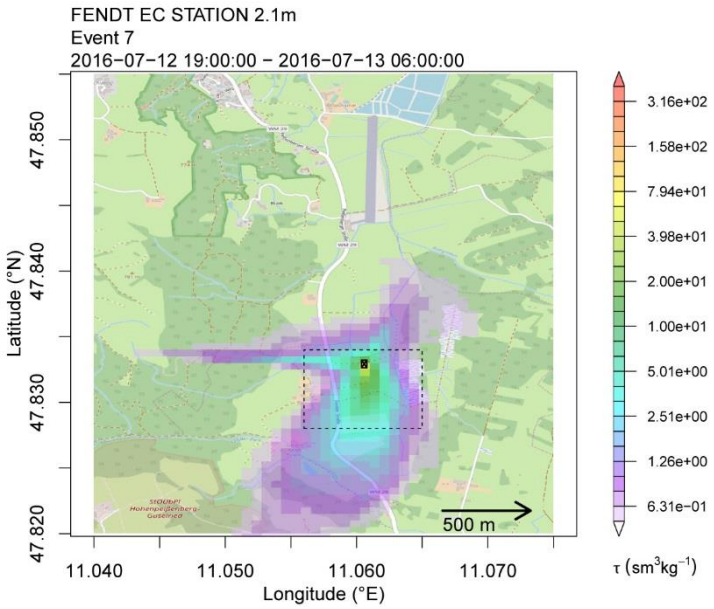
FENDT EC STATION 2.1m
Event 7
2016-07-12 19:00:00 – 2016-07-13 06:00:00
Latitude (°N)
47.820
47.830
47.840
47.850
11.040
11.050
11.060
11.070
Longitude (°E)
500 m
3.16e+02
1.58e+02
7.94e+01
3.98e+01
2.00e+01
1.00e+01
5.01e+00
2.51e+00
1.26e+00
6.31e-01
τ (sm3kg-1)

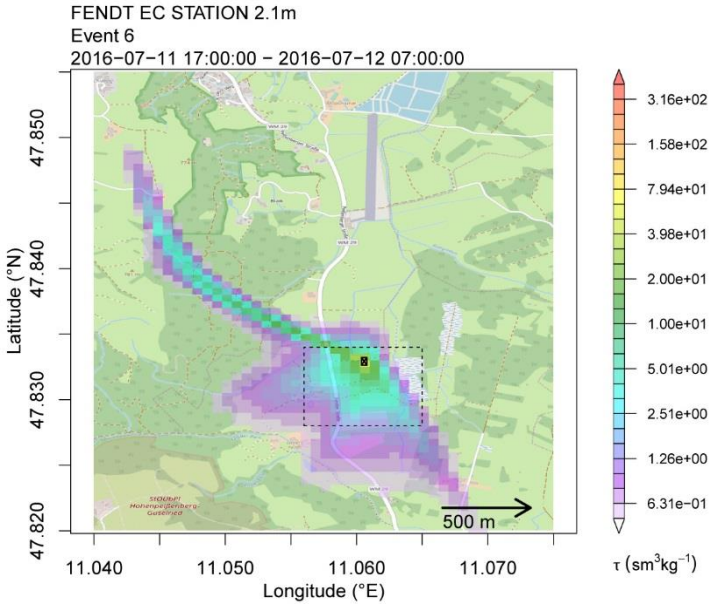
FENDT EC STATION 2.1m
Event 6
2016-07-11 17:00:00 – 2016-07-12 07:00:00
Latitude (°N)
47.850
47.840
47.830
47.820
11.040
11.050
11.060
11.070
Longitude (°E)
500 m
3.16e+02
1.58e+02
7.94e+01
3.98e+01
2.00e+01
1.00e+01
5.01e+00
2.51e+00
1.26e+00
6.31e-01
τ (sm3kg−1)

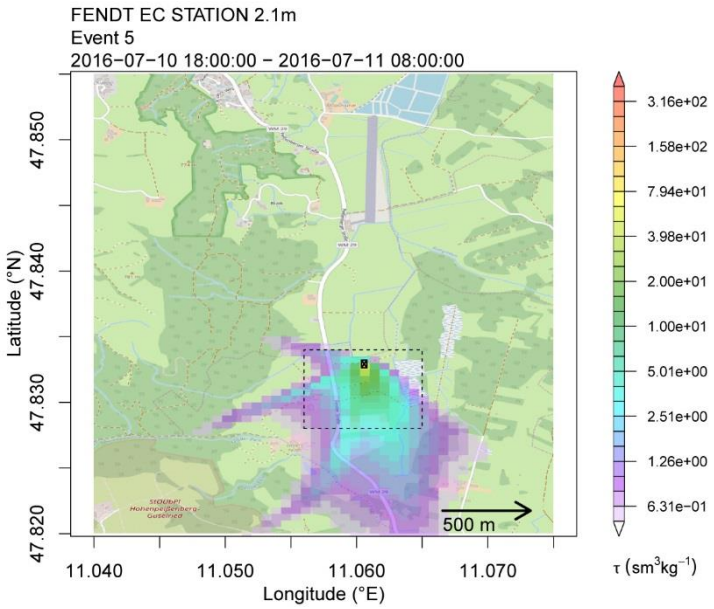
FENDT EC STATION 2.1m
Event 5
2016-07-10 18:00:00 – 2016-07-11 08:00:00
Latitude (°N)
47.850
47.840
47.830
47.820
11.040
11.050
11.060
11.070
Longitude (°E)
500 m
3.16e+02
1.58e+02
7.94e+01
3.98e+01
2.00e+01
1.00e+01
5.01e+00
2.51e+00
1.26e+00
6.31e-01
τ (sm3kg−1)

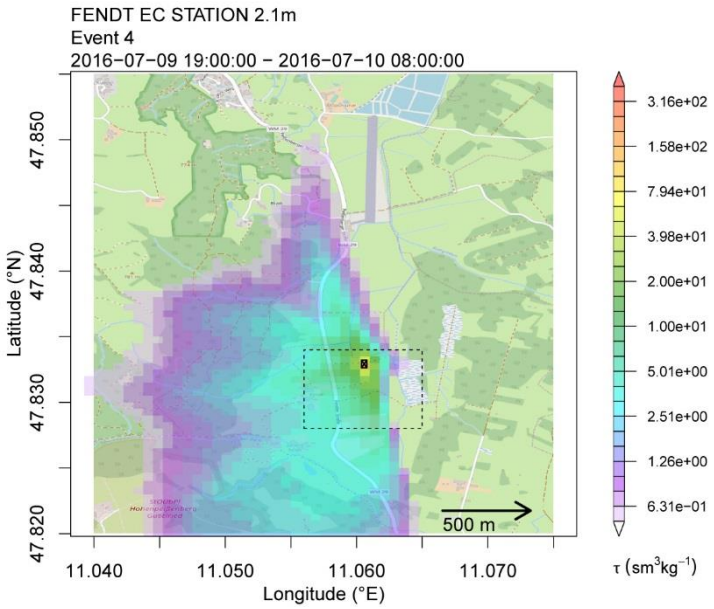
FENDT EC STATION 2.1m
Event 4
2016-07-09 19:00:00 – 2016-07-10 08:00:00
Latitude (°N)
47.850
47.840
47.830
47.820
11.040
11.050
11.060
11.070
Longitude (°E)
500 m
3.16e+02
1.58e+02
7.94e+01
3.98e+01
2.00e+01
1.00e+01
5.01e+00
2.51e+00
1.26e+00
6.31e-01
τ (sm3kg−1)

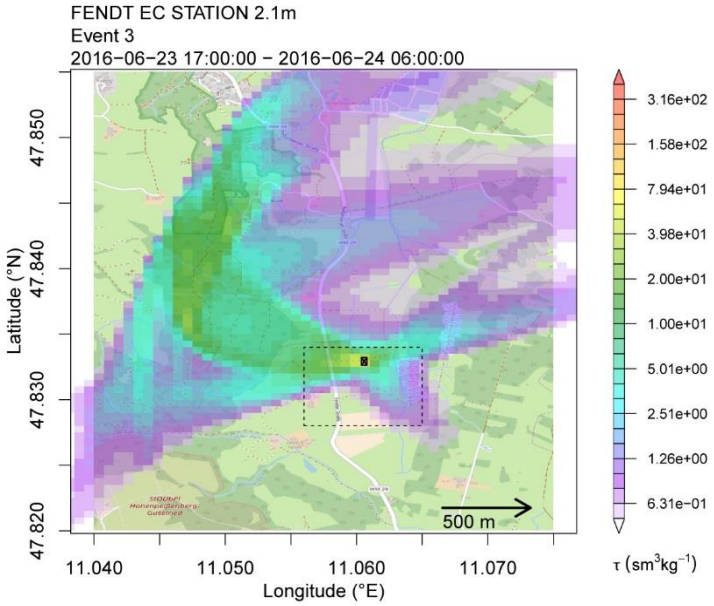
FENDT EC STATION 2.1m
Event 3
2016-06-23 17:00:00 - 2016-06-24 06:00:00
Latitude (°N)
47.850
47.840
47.830
47.820
11.040
11.050
11.060
11.070
Longitude (°E)
500 m
3.16e+02
1.58e+02
7.94e+01
3.98e+01
2.00e+01
1.00e+01
5.01e+00
2.51e+00
1.26e+00
6.31e-01
τ (sm3kg-1)

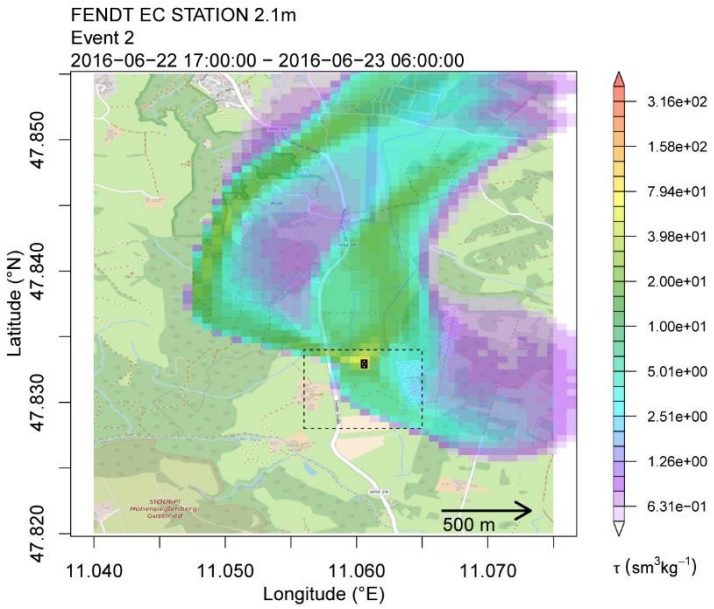
FENDT EC STATION 2.1m
Event 2
2016-06-22 17:00:00 - 2016-06-23 06:00:00
Latitude (°N)
47.850
47.840
47.830
47.820
11.040
11.050
11.060
11.070
Longitude (°E)
500 m
3.16e+02
1.58e+02
7.94e+01
3.98e+01
2.00e+01
1.00e+01
5.01e+00
2.51e+00
1.26e+00
6.31e-01
τ (sm3kg-1)

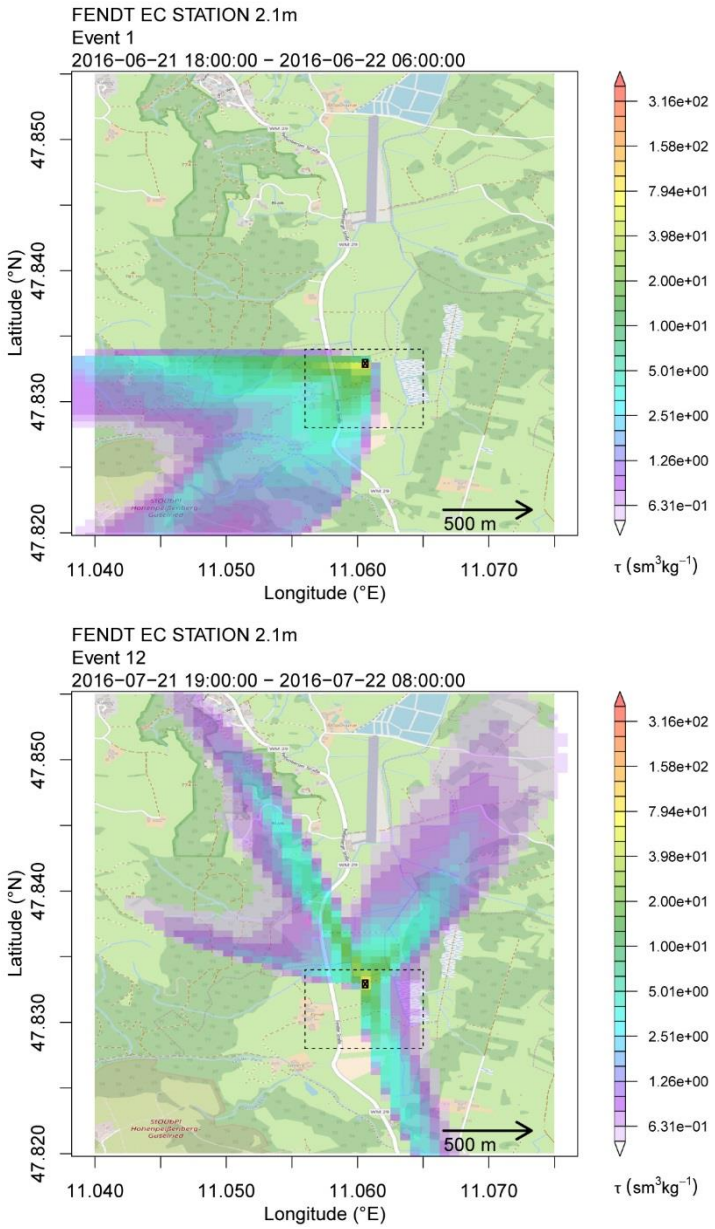

SI Figure 11 Individual footprints of the 12 accumulation events

1. References

Harris, E., Henne, S., Hüglin, C., Zellweger, C., Tuzson, B., Ibraim, E., Emmenegger, L., and Mohn, J.: Tracking nitrous oxide emission processes at a suburban site with semicontinuous, in situ measurements of isotopic composition, Journal of Geophysical Research: Atmospheres, 122, 1850-1870, 10.1002/2016JD025906, 2017.

Keeling, C. D.: The Concentration and Isotopic Abundances of Atmospheric Carbon Dioxide in Rural Areas, Geochimica Et Cosmochimica Acta, 13, 322-334, Doi 10.1016/0016-7037(58)90033-4, 1958.

Keeling, C. D.: The Concentration and Isotopic Abundances of Carbon Dioxide in Rural and Marine Air, Geochim. Cosmochim. Acta, 24, 277-298, Doi 10.1016/0016-7037(61)90023-0, 1961.

Koba, K., Osaka, K., Tobari, Y., Toyoda, S., Ohte, N., Katsuyama, M., Suzuki, N., Itoh, M., Yamagishi, H., Kawasaki, M., Kim, S. J., Yoshida, N., and Nakajima, T.: Biogeochemistry of nitrous oxide in groundwater in a forested ecosystem elucidated by nitrous oxide isotopomer measurements, Geochim. Cosmochim. Acta, 73, 3115-3133, 10.1016/j.gca.2009.03.022, 2009.

Lewicka-Szczebak, D., Augustin, J., Giesemann, A., and Well, R.: Quantifying N_2O reduction to N_2 based on N_2O isotopocules - validation with independent methods (helium incubation and ^{15}N gas flux method), Biogeosciences, 14, 10.5194/bg-14-711-2017, 2017.

Miller, J. B., and Tans, P. P.: Calculating isotopic fractionation from atmospheric measurements at various scales, Tellus (B Chem. Phys. Meteorol.), 55, 207-214, 10.1034/j.1600-0889.2003.00020.x, 2003.